RTAXS TAMU Single Event Latch-up Test Report

July 12, 2006

J.J. Wang and S. Rezgui
(650) 318-4576
jih-jong.wang@actel.com

I. Summary

RTAX2000S devices biased to nominal or +10% V_{CC} are tested for SEL at elevated temperature approximately 125°C. Heavy ions with effective LET up to 117.2 MeV•cm^2/mg are used for irradiation. No SEL were observed in any test run. Non-critical SEDR (single event dielectric rupture) was observed in one DUT +10% biased and irradiated by Au-ions. This SEDR level is significantly lower than previous generations of antifuse-FPGA products.

II. Test Objective

The objective is to test the SEL susceptibility of the RTAX2000S device operating at elevated temperature up to 125°C. Previously obtained room-temperature data show that this device is immune to SEL for LET up to 100 MeV•cm^2/mg. This test also wants to extend the data range to cover higher LET.

II. Device Under Test

The specific information defining the DUT is listed in Table I.

Table I DUT Information

Device	RTAX2000S
Package	CQ352
Foundry	UMC
Technology	0.15 µm CMOS
Die-Lot/Serial Number	D1L9R1: 73026 D1KHN1: 79023, 79102
Quantity Tested	3
IO Configuration	LVTTL
Design	SR_1000_4P_70_sp1

III. Testing

The DUT design is composed of four (4) 1000-bit shift registers; two shift registers share a HCLK and the other two registers share a RCLK. During each run, the input data pattern is always checkerboard clocked at 1 MHz. The functionality of the DUT is monitored by an oscilloscope. Fig. 1 shows a snap shot of the waveform. Although the waveform shows strong reflection and ringing, the determination of the functionality is still a clear cut. The DUT power-supply currents, I_{CCI} and I_{CCA}, are also monitored and recorded throughout each run. The DUT biases (V_{CCI}/V_{CCA}) for each run are either nominal (3.3 V/1.5 V) or +10% (3.6 V/1.65 V).

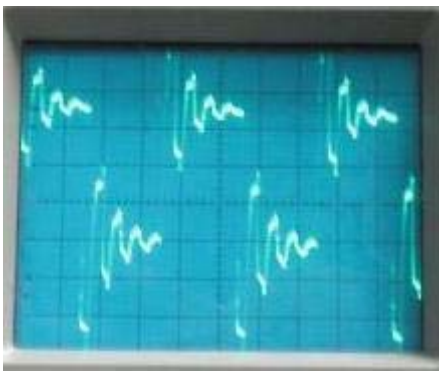

Fig.1 Oscilloscope capture of a checkerboard pattern during heavy-ion irradiation, showing the functionality of the DUT.

To achieve the elevated temperature on the DUT, a resistor heater and a RTD sensor are taped to the back of the package. The temperature on the die is correlated with the temperature on the back of the package by using a

dummy device with sensors on both the die and the back of the package. Approximately 125°C (±5%) is maintained during each run of heavy-ion irradiation.

15-MeV/nucleon Au and Xe ions are used for irradiation. As shown in Table II, the effective LET varies from 49.3 to 117.2 MeV•cm^2/mg, and the effective fluence for each run is approximately 1×10^7 ions/cm^2.

IV. Results and Discussions

Table II shows the data log; it records all the relevant testing parameters for each run. The waveform displayed on the oscilloscope confirms that the DUT is functional throughout heavy-ion irradiation in every run.

Fig. 2 to 18 shows the plot of in-flux power-supply currents, I_{CCI} and I_{CCA}, for each run. There is no indication of single event latch-up (SEL) in any run. Fig. 8 and Fig. 10 (Run 2 and Run 4) show current jumps of several mA in DUT79023 under +10% over-bias during Au-ions irradiations. These current jumps are permanent because recycling the power doesn't recover the DUT to the current state before the jump. This abnormality shows the typical characteristics of single event dielectric rupture (SEDR) in antifuse. Only the current jumps in I_{CCA} are directly related to SEDR because any antifuse can only be biased by V_{CCA}; the I_{CCI} current jumps are induced after the leakage occurred in the circuit. These SEDR events occurred in non-critical path so that the functionality was maintained. Nevertheless, these data show that, compared to previous generations of antifuse FPGAs, RTAXS is less susceptible to SEDR; the onset LET is so high that the FIT rate should be negligible.

Table Test Log

Run	DUT	Bias (V) V_{CCI}/V_{CCA}	Temp (°C)	Ion	LET MeV•cm^2/mg	Tilt	Flux Ions/cm^2/s	Fluence Ions/cm^2	File Name	Comments
1	79023	3.7/1.7	125	Au	82.8	0	NA	NA	79023Au1	Run aborted
2	79023	3.7/1.7	125	Au	82.8	0	8.71E+04	9.97E+06	79023Au2	Functional
3	79023	3.3/1.5	125	Au	117.2	45	1.50E+05	9.97E+06	79023Au3	Functional
4	79023	3.6/1.65	125	Au	117.2	45	1.67E+05	1.00E+07	79023Au4	Functional
5	79023	3.3/1.5	125	Au	82.8	0	1.73E+05	1.00E+07	79023Au5	Functional
6	73026	3.3/1.5	125	Au	82.8	0	1.14E+05	9.99E+06	73026Au1	Functional
7	73026	3.6/1.65	125	Au	82.8	0	1.19E+05	9.96E+06	73026Au2	Functional
8	73026	3.3/1.5	125	Au	117.2	45	1.21E+05	9.96E+06	73026Au3	Functional
9	73026	3.6/1.65	125	Au	117.2	45	1.23E+05	1.00E+07	73026Au4	Functional
10	79102	3.3/1.5	125	Au	82.8	0	1.51E+05	1.00E+07	79102Au1	Functional
11	79102	3.6/1.65	125	Au	82.8	0	1.42E+05	9.98E+06	79102Au2	Functional
12	79102	3.3/1.5	125	Au	117.2	45	1.18E+05	1.00E+07	79102Au3	Functional
13	79102	3.6/1.65	125	Au	117.2	45	7.88E+04	9.99E+06	79102Au4	Functional
14	79102	3.6/1.65	125	Xe	69.8	45	1.12E+05	9.97E+06	79102Xe1	Functional
15	79102	3.6/1.65	125	Xe	49.3	0	1.12E+05	9.94E+06	79102Xe2	Functional
16	73026	3.6/1.65	125	Xe	49.3	0	1.11E+05	1.00E+07	73026Xe1	Functional
17	73026	3.6/1.65	125	Xe	69.8	45	1.04E+05	1.00E+07	73026Xe2	Functional
18	79023	3.6/1.65	125	Xe	49.3	0	1.05E+05	9.96E+06	79023Xe1	Functional
19	79023	3.6/1.65	125	Xe	69.8	45	1.12E+04	1.00E+07	79023Xe2	Functional

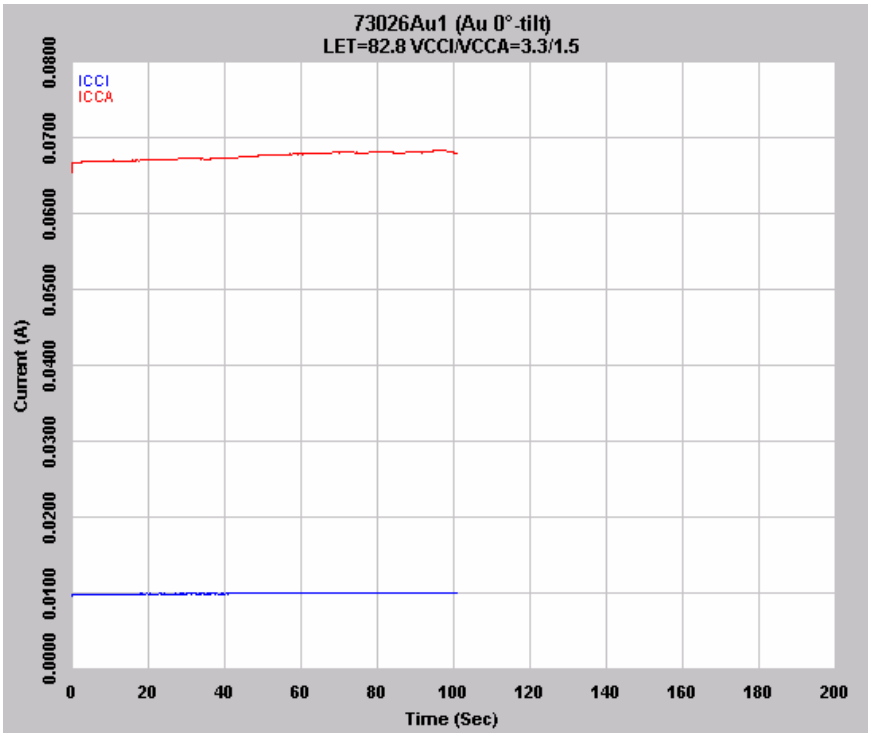

Fig. 2 Plot showing in-flux power supply currents (I_{CCI} and I_{CCA}) of DUT73026 irradiated by Au-ions with 0° tilt; effective LET = 82.8 MeV•cm^2/mg; V_{CCI}/V_{CCA} = 3.3 V/1.5 V

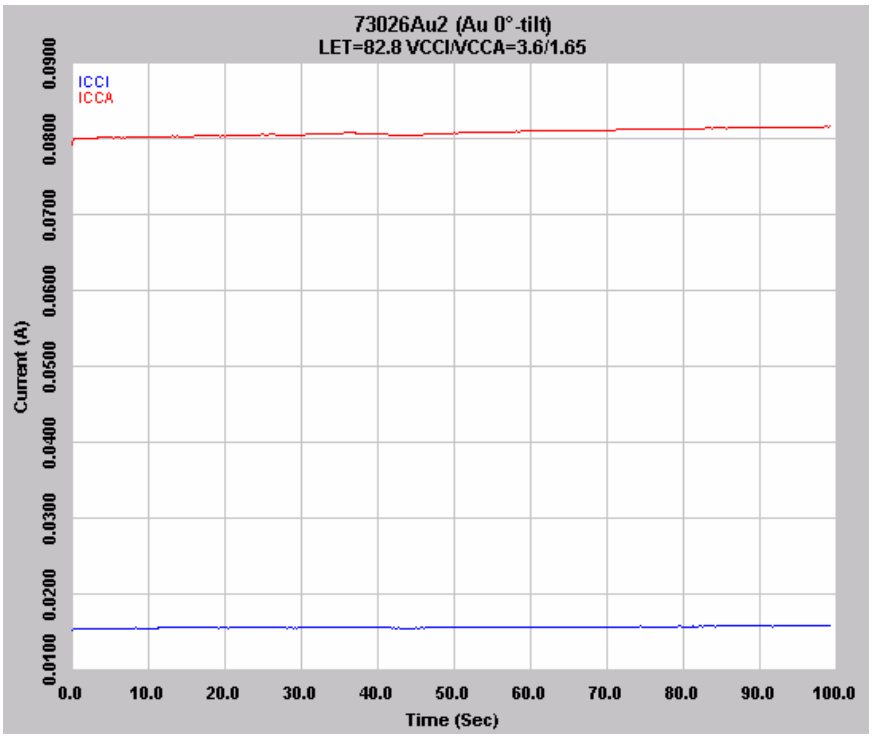

Fig. 3 Plot showing in-flux power supply currents (I_{CCI} and I_{CCA}) of DUT73026 irradiated by Au-ions with 0° tilt; effective LET = 82.8 MeV•cm^2/mg; V_{CCI}/V_{CCA} = 3.6 V/1.65 V.

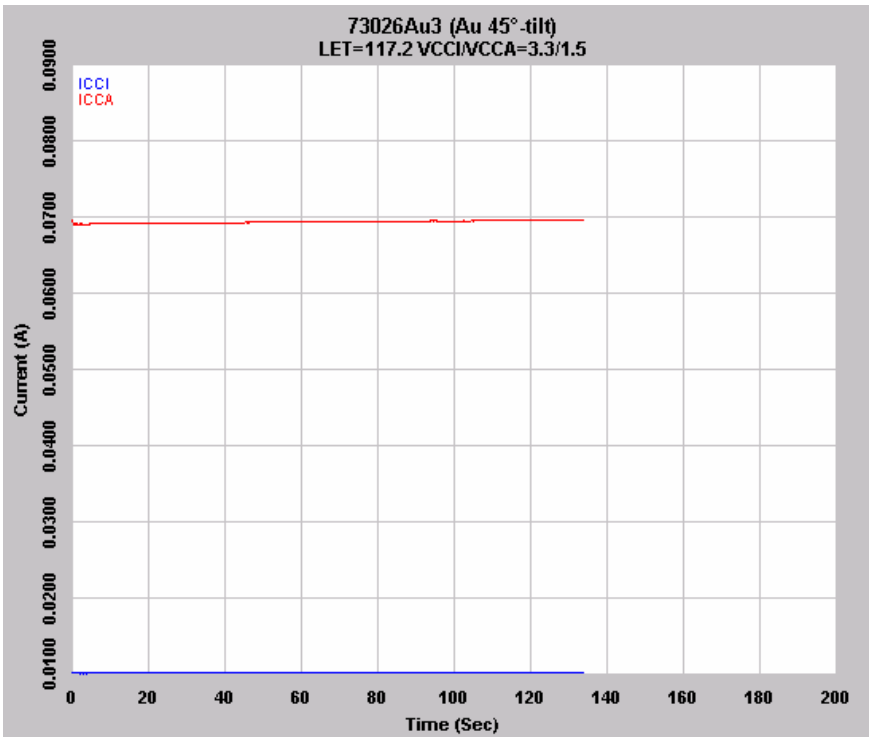

Fig. 4 Plot showing in-flux power supply currents (I_{CCI} and I_{CCA}) of DUT73026 irradiated by Au-ions with 45° tilt; effective LET = 117.2 MeV•cm^2/mg; V_{CCI}/V_{CCA} = 3.3 V/1.5 V.

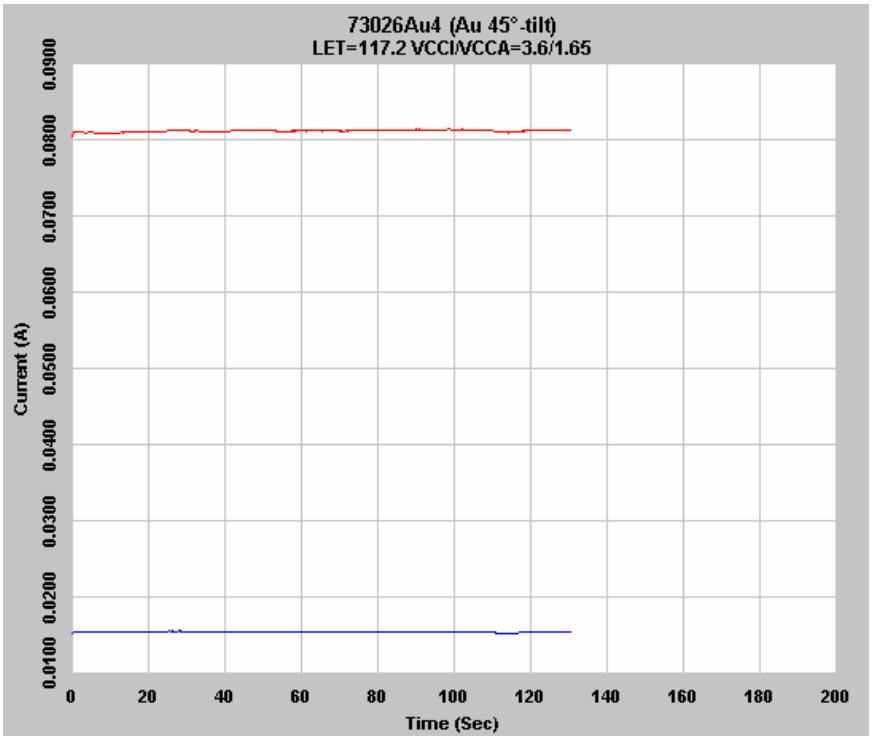

Fig. 5 Plot showing in-flux power supply currents (I_{CCI} and I_{CCA}) of DUT73026 irradiated by Au-ions with 45° tilt; effective LET = 117.2 MeV•cm^2/mg; V_{CCI}/V_{CCA} = 3.6 V/1.65 V.

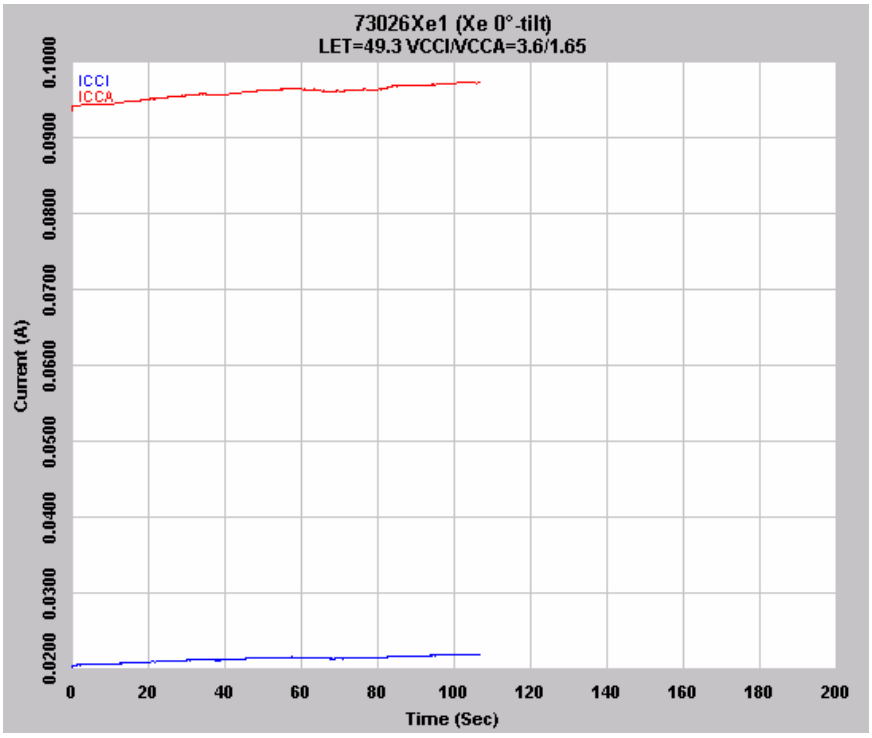

Fig. 6 Plot showing in-flux power supply currents (I_{CCI} and I_{CCA}) of DUT73026 irradiated by Xe-ions with 0° tilt; effective LET = 49.3 MeV•cm^2/mg; V_{CCI}/V_{CCA} = 3.6 V/1.65 V.

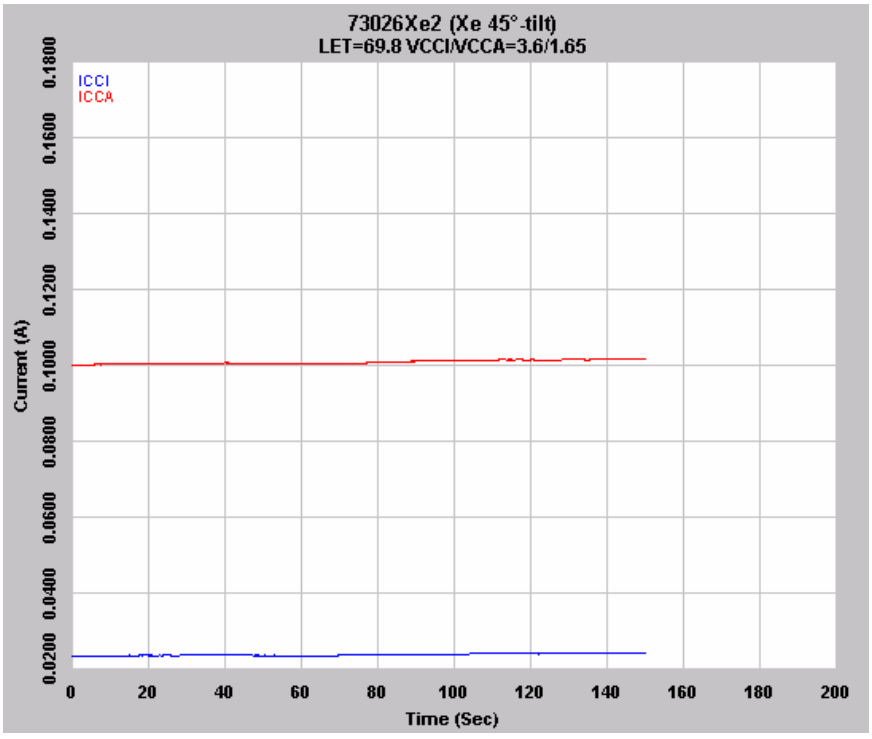

Fig. 7 Plot showing in-flux power supply currents (I_{CCI} and I_{CCA}) of DUT73026 irradiated by Xe-ions with 45° tilt; effective LET = 69.8 MeV•cm^2/mg; V_{CCI}/V_{CCA} = 3.6 V/1.65 V.

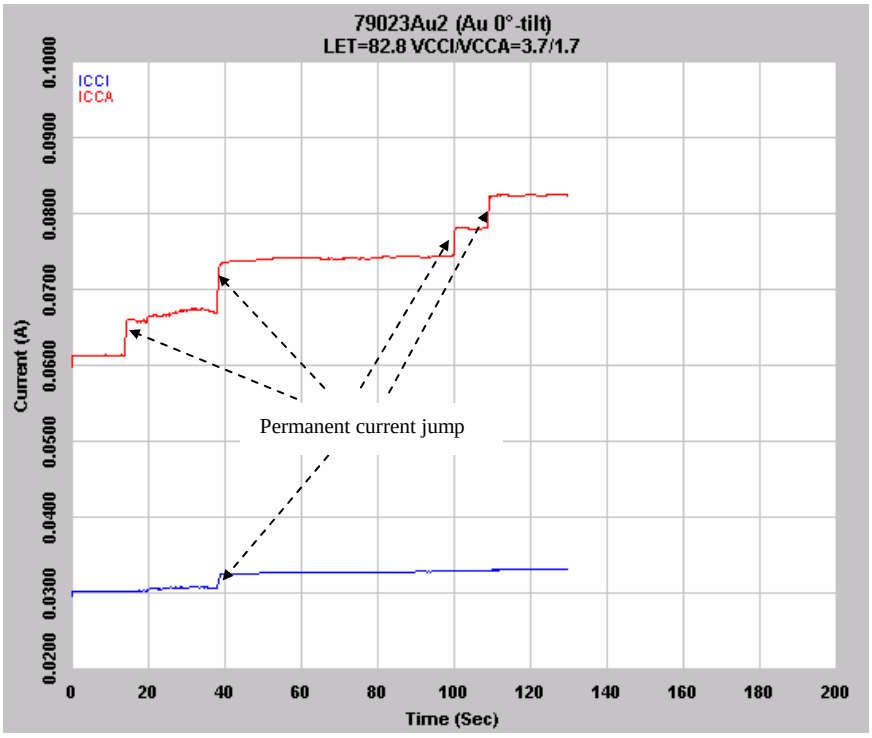

Fig. 8 Plot showing in-flux power supply currents (I_{CCI} and I_{CCA}) of DUT79023 irradiated by Au-ions with 0° tilt; effective LET = 82.8 MeV•cm^2/mg; V_{CCI}/V_{CCA} = 3.7 V/1.7 V.

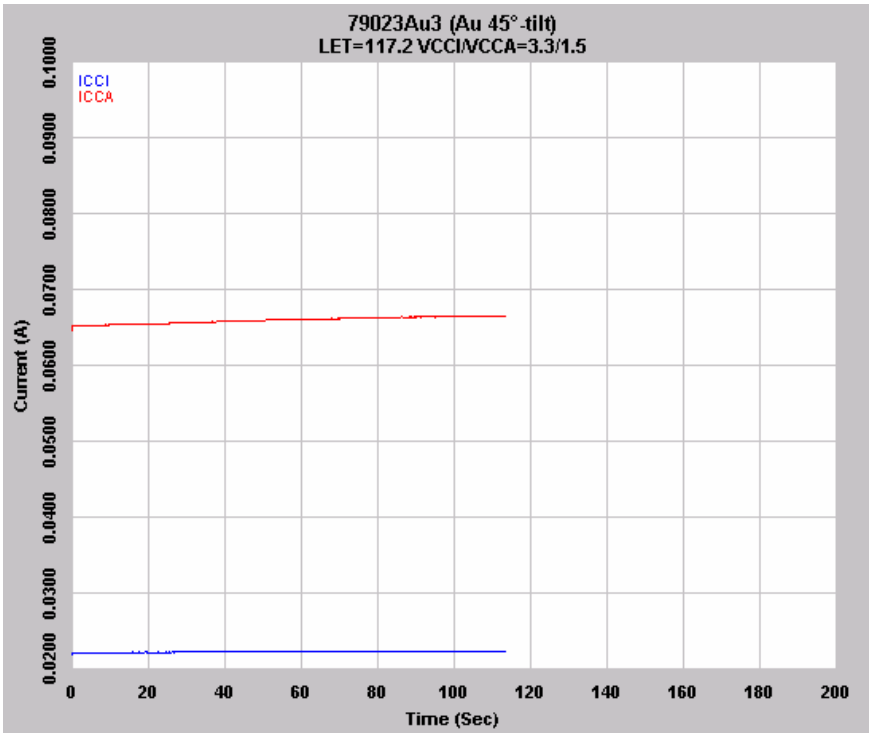

Fig. 9 Plot showing in-flux power supply currents (I_{CCI} and I_{CCA}) of DUT79023 irradiated by Au-ions with 45° tilt; effective LET = 117.2 MeV•cm^2/mg; V_{CCI}/V_{CCA} = 3.3 V/1.5 V.

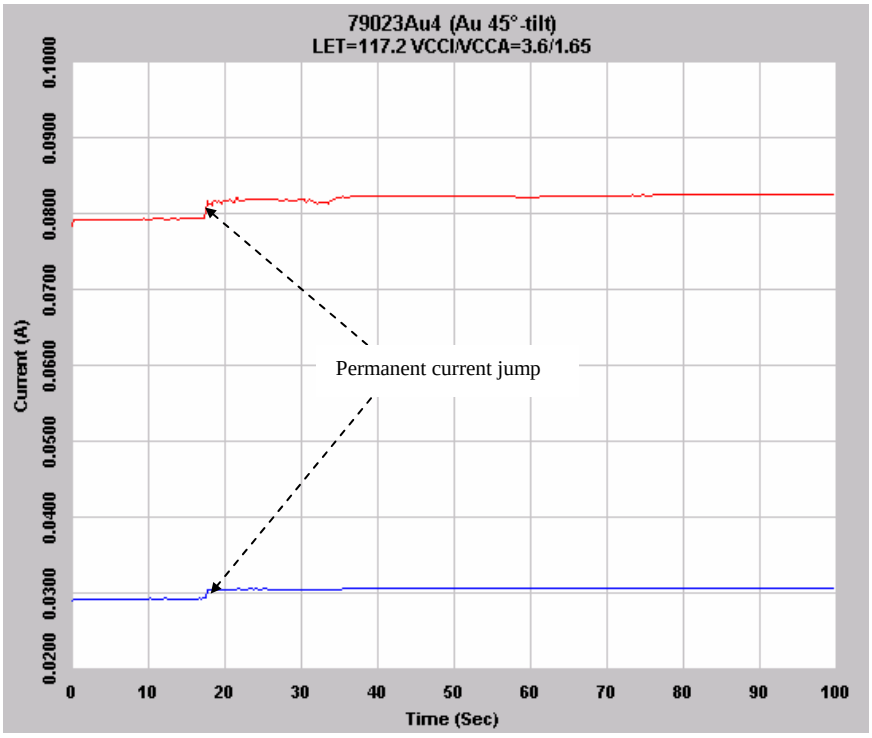

Fig. 10 Plot showing in-flux power supply currents (I_{CCI} and I_{CCA}) of DUT79023 irradiated by Au-ions with 45° tilt; effective LET = 117.2 MeV•cm^2/mg; V_{CCI}/V_{CCA} = 3.6 V/1.65 V.

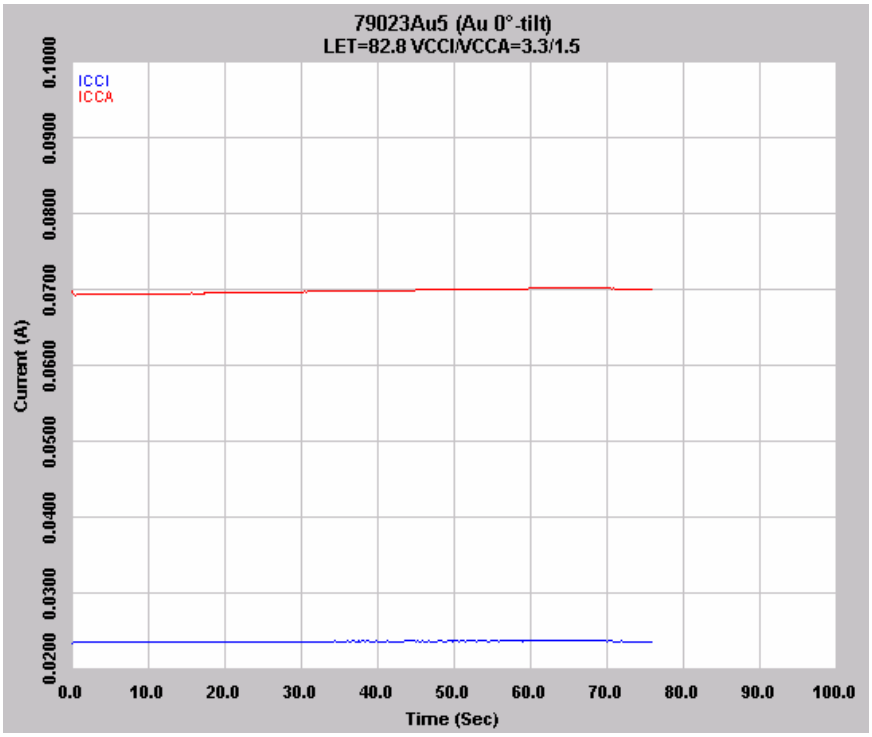

Fig. 11 Plot showing in-flux power supply currents (I_{CCI} and I_{CCA}) of DUT79023 irradiated by Au-ions with 0° tilt; effective LET = 82.8 MeV•cm^2/mg; V_{CCI}/V_{CCA} = 3.3 V/1.5 V.

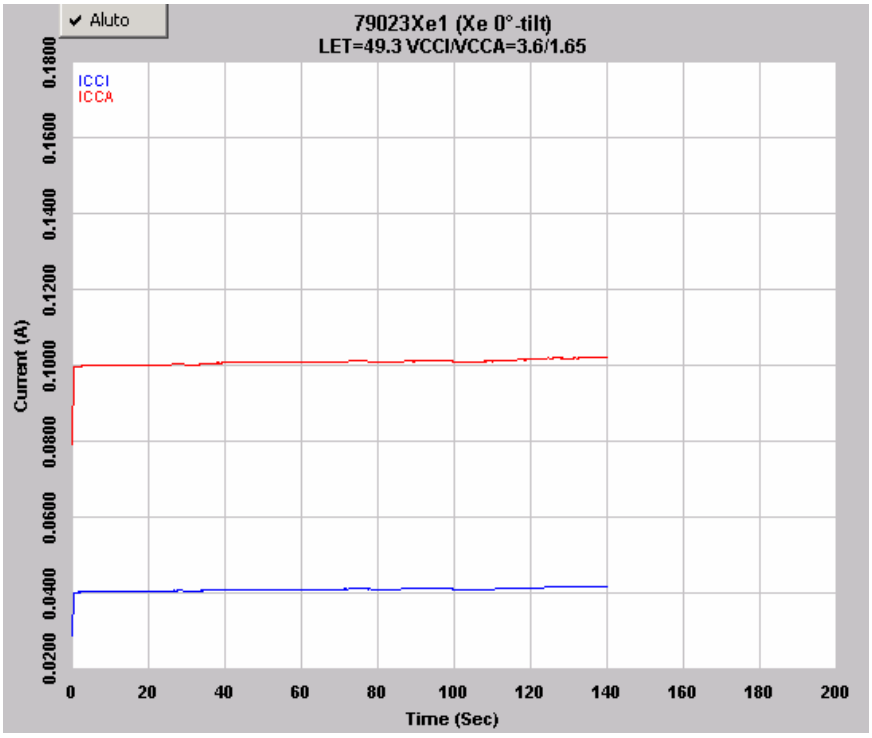

Fig. 12 Plot showing in-flux power supply currents (I_{CCI} and I_{CCA}) of DUT79023 irradiated by Xe-ions with 0° tilt; effective LET = 49.3 MeV•cm^2/mg; V_{CCI}/V_{CCA} = 3.6 V/1.65 V.

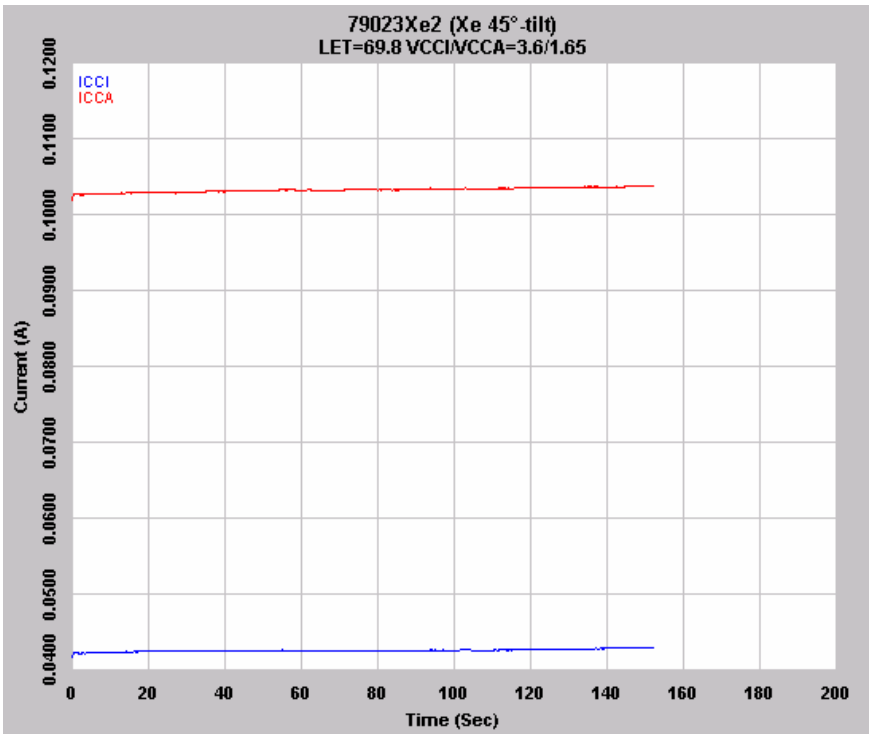

Fig. 13 Plot showing in-flux power supply currents (I_{CCI} and I_{CCA}) of DUT79023 irradiated by Xe-ions with 45° tilt; effective LET = 69.8 MeV•cm^2/mg; V_{CCI}/V_{CCA} = 3.6 V/1.65 V.

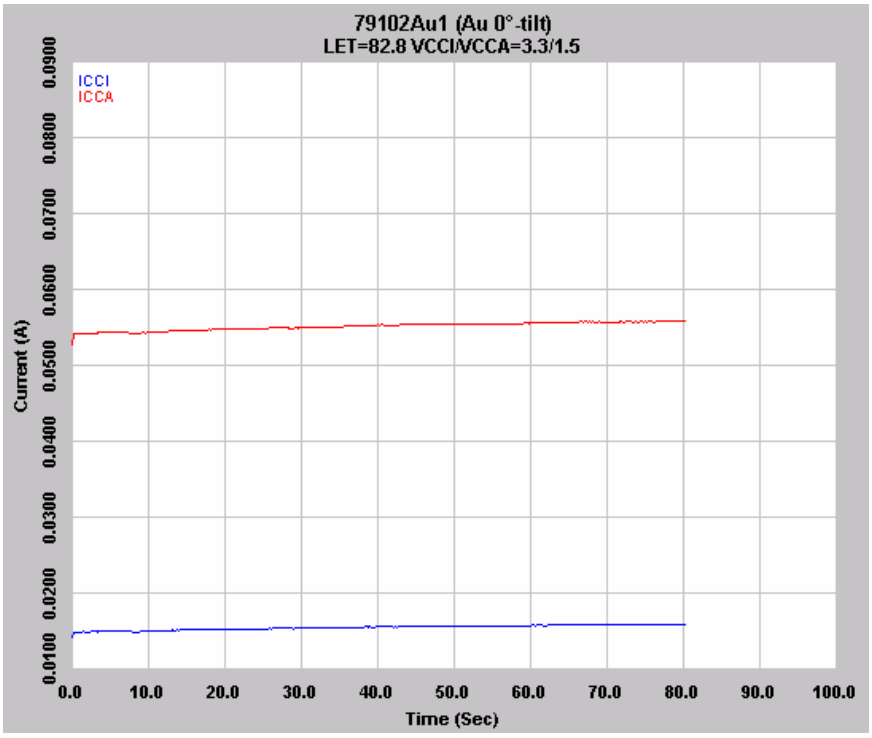

Fig. 14 Plot showing in-flux power supply currents (I_{CCI} and I_{CCA}) of DUT79102 irradiated by Au-ions with 0° tilt; effective LET = 82.8 MeV•cm^2/mg; V_{CCI}/V_{CCA} = 3.3 V/1.5 V.

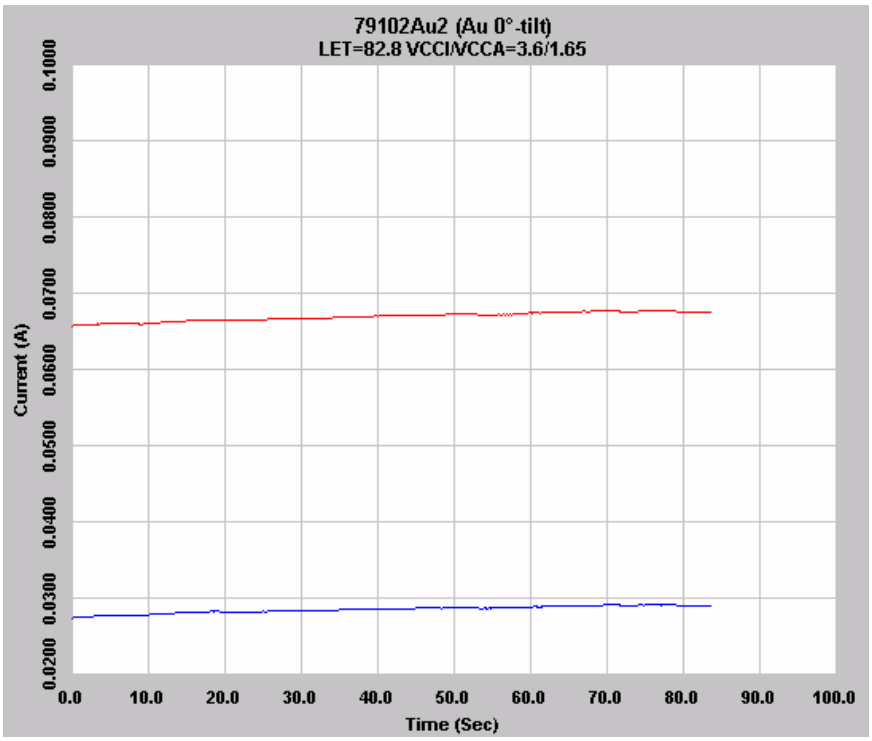

Fig. 15 Plot showing in-flux power supply currents (I_{CCI} and I_{CCA}) of DUT79102 irradiated by Au-ions with 0° tilt; effective LET = 82.8 MeV•cm^2/mg; V_{CCI}/V_{CCA} = 3.6 V/1.65 V.

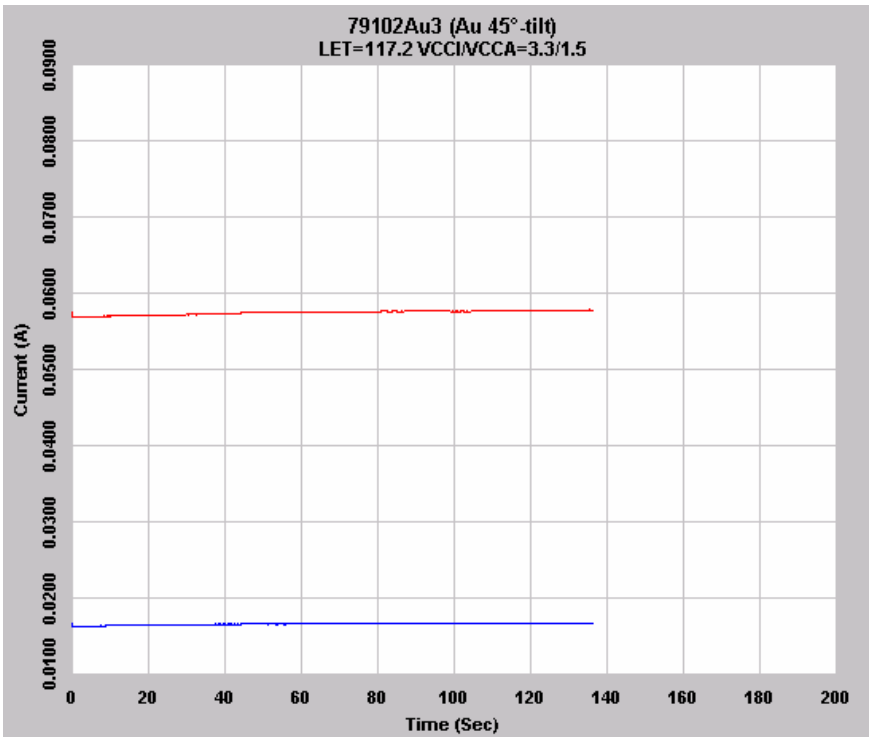

Fig. 16 Plot showing in-flux power supply currents (I_{CCI} and I_{CCA}) of DUT79102 irradiated by Au-ions with 45° tilt; effective LET = 117.2 MeV•cm^2/mg; V_{CCI}/V_{CCA} = 3.3 V/1.5 V.

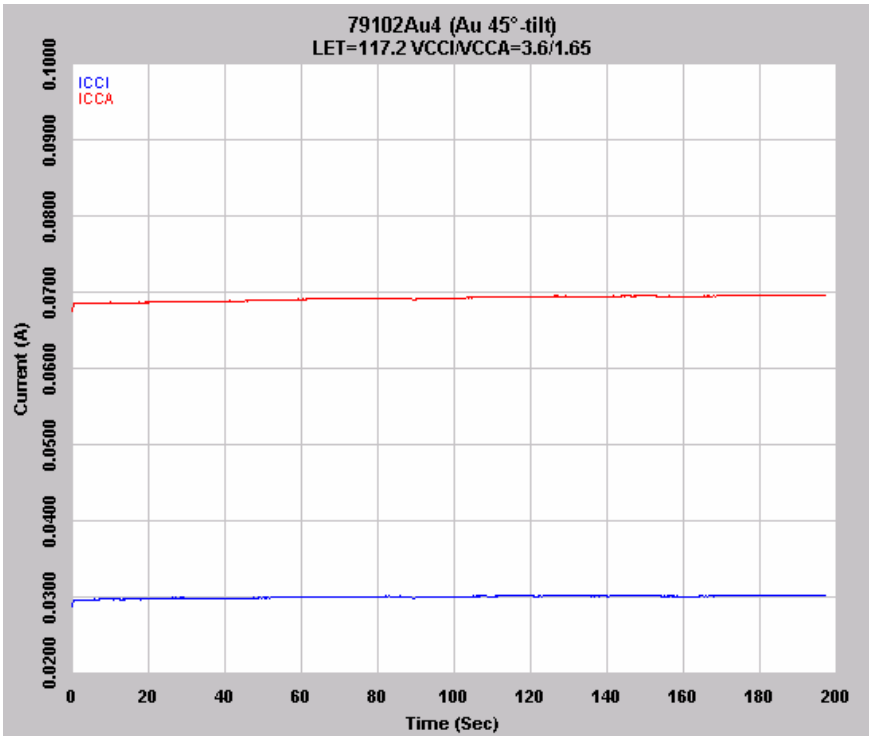

Fig. 17 Plot showing in-flux power supply currents (I_{CCI} and I_{CCA}) of DUT79102 irradiated by Au-ions with 45° tilt; effective LET = 117.2 MeV•cm^2/mg; V_{CCI}/V_{CCA} = 3.6 V/1.65 V.

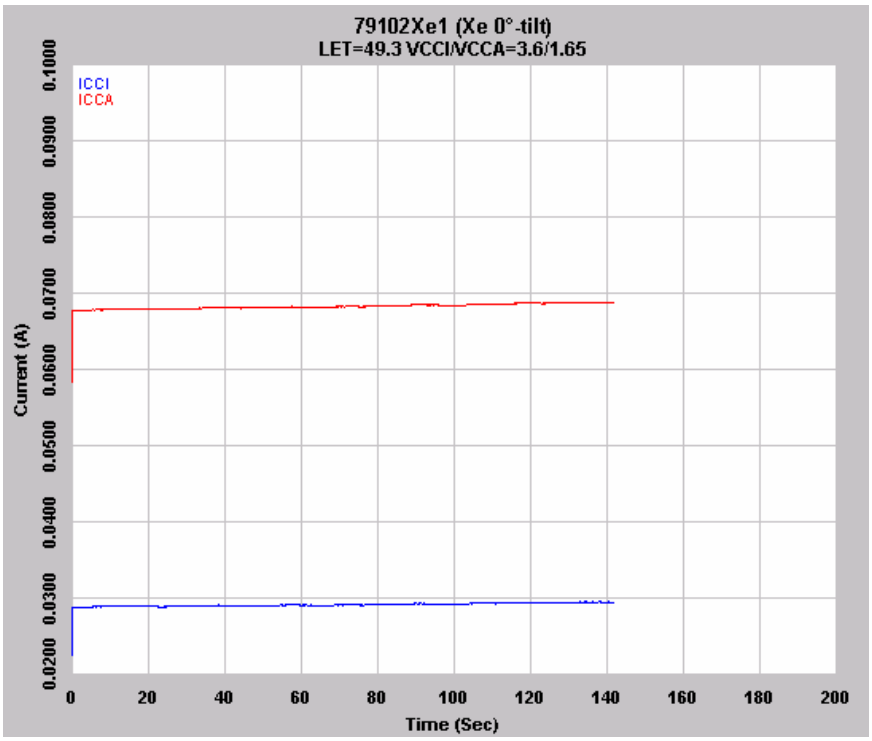

Fig. 18 Plot showing in-flux power supply currents (I_{CCI} and I_{CCA}) of DUT79102 irradiated by Xe-ions with 0° tilt; effective LET = 49.3 MeV•cm^2/mg; V_{CCI}/V_{CCA} = 3.6 V/1.65 V.

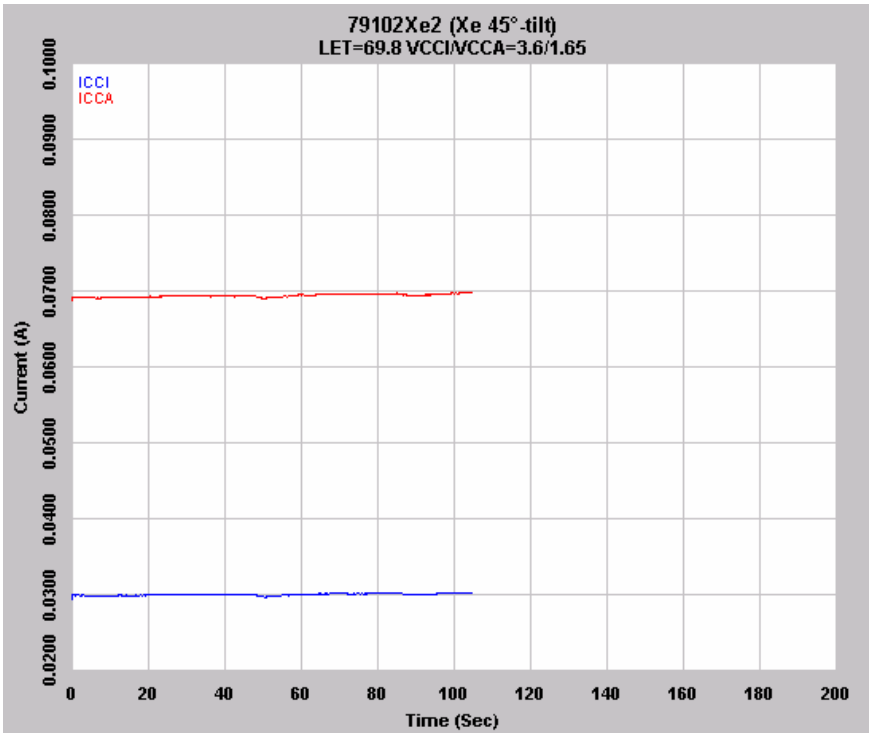

Fig. 19 Plot showing in-flux power supply currents (I_{CCI} and I_{CCA}) of DUT79102 irradiated by Xe-ions with 45° tilt; effective LET = 69.8 MeV•cm^2/mg; V_{CCI}/V_{CCA} = 3.6 V/1.65 V.